Rate of seismic deformation in the Gulf of Aqaba inferred from moment-tensor summation

SATTAM ALMADANI

Geology and Geophysics Department, College of Science, King Saud University, Riyadh 11451, Kingdom of Saudi Arabia (salmadani@ksu.edu.sa)

Received: April 14, 2020; Revised: August 19, 2020; Accepted: October 11, 2020

ABSTRACT

This study aims to quantify the rate of coseismic deformation in the Gulf of Aqaba. Earthquake catalogue, Gutenberg-Richter relationship and fault plane solutions were integrated to measure the size and shape of deformation using the moment-tensor summation technique. First, the Gutenberg-Richter relationship was established using seismicity data from the period of 1964–2019. Then, the moment-tensor summation based on 44 focal mechanism solutions was used to calculate the shape of deformation. The eigenvalues of moment-tensor reflect the diversity of focal mechanism solutions that alternate from normal to strike-slip fault styles in the deformation zone. The analysis reveals a dominant shear deformation in the Gulf of Aqaba that extends in a direction of N42.2°E at a rate of 2.6 ± 0.04 mm yr^{-1} and shortens in the direction of N305.2°E at a rate of 2.0 ± 0.02 mm yr^{-1}. These results suggest that the active deformation occurring in the Gulf of Aqaba is due to the relative tectonic movements between the Arabian and African plates, as well as Sinai subplate.

Keywords: focal mechanism, Gulf of Aqaba, Gutenberg-Richter law, moment magnitude, crustal deformation

1. INTRODUCTION

The Dead Sea fault is one of the transform plate boundaries in the world, formed by the relative tectonic movements of the African and Arabian plates, as well as the key role of Sinai subplate. The Gulf of Aqaba represents a transition zone that connects the Dead Sea fault with a sinistral offset and the Red Sea rifting (*Garfunkel, 1981*; *Salamon et al., 1996*). The Gulf of Aqaba is formed by three structural basins that are typically bounded to the east and west by longitudinal faults (*Ben-Avraham, 1985*). The main fault is characterized at several locations by left-handed stepovers that continue as parallel faults with sinistral displacement, generating pull-apart basins (*Daggett et al., 1986*). The longitudinal basins and the en-echelon faults are shown later. Previous studies have used various datasets to indicate that this movement initiated during the late Miocene at ~14–11 Ma (*Garfunkel, 1981*). The slip rate based on geodetic estimates indicates left-lateral deformation at 4.4 ± 0.3 mm yr^{-1} along the Gulf of Aqaba-Dead Sea transform

fault (*Mahmoud et al., 2005*), whereas the sinistral motion of 5.6 ± 10 mm yr^{-1} was determined for the southernmost segment of the Aqaba fault (*McClusky et al., 2003*). The low recurrence rate of earthquakes with magnitudes greater than six implies that the total horizontal slip rate of 2–4 mm yr^{-1} is accommodated to the north of the western side of the Gulf of Aqaba (*Makovsky et al., 2008*). A kinematic study by *Jestin et al. (1994)* indicated that tectonic processes produced a seismogenic zone characterized by extensional-to-shear deformation, which revealed that seismicity in the Gulf is due to relative plate motion between the African and Arabian plates. This relative plate motion is illustrated in Fig. 1.

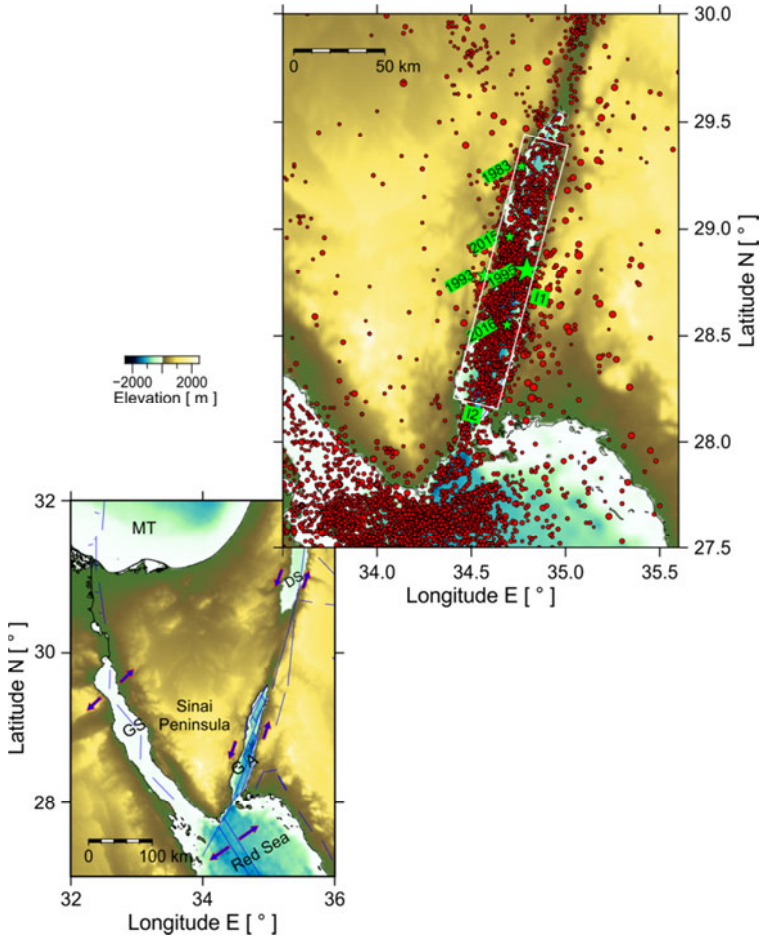

Fig. 1. Map of seismicity in the Gulf of Aqaba from 1964–2019 (circles), showing distinctive earthquake sequences that occurred in 1983, 1993, 1995, 2015, and 2016 (stars). The arrows reflect the tectonic environments in the Gulf of Aqaba, Gulf of Suez, and the northernmost part of the Red Sea. MT - Mediterranean Sea, GS - Gulf of Suez, GA - Gulf of Aqaba, DS - Dead Sea. The white rectangle delineates the seismogenic deformation zone.

The Gulf of Aqaba has experienced several earthquake sequences that are clustered both in space and time, indicating localization of crustal deformation within the Earth's crust (*Abdel-Fattah et al., 2006*). Seismicity in the Gulf of Aqaba from 1964–2019 is shown in Fig. 1. The 1995 earthquake sequence with moment magnitude M_w of 7.2 was the most destructive earthquake in the Gulf since the beginning of the century (*Salamon et al., 1996*). The focal mechanisms of moderate-to-large size earthquakes reveal normal to strike-slip faulting mechanisms (*Abdel-Fattah et al., 2006*, *Abd el-All and Badreldin, 2016*, *Almadani, 2017*). Moreover, seismic tomography derived by *El Khrepy et al. (2016)* indicated no continued extension from the Red Sea, implying a transition of crustal types towards the north.

Accurate estimates of the velocity and strain tensors of seismogenic deformation are vital for characterizing active crustal deformation within seismogenic zones and determining the seismic hazard of active regions. Integration between geological, geodetic, and seismological data is crucial for obtaining more stable and constrained estimates of the strain rate. However, the geologically derived strain rate depends on quantitative geological data of the study area, which are not always available. Moreover, although the geodetic strain considers the total active deformation, it cannot distinguish seismic components from aseismic ones (*Visini et al., 2010*). Moreover, it remains unclear whether geodetic data can be extrapolated to longer periods owing to the short instrumental data record (*Papanikolaou et al., 2005*). Due to these limitations of geological and geodetic observations, the seismological approach remains valuable for quantifying the rate of active crustal deformation through available historical and instrumental data.

Different approaches have been applied to estimate coseismic deformation (e.g., *Jackson and McKenzie, 1988*; *Kiratzi, 1991, 1993*; *Papazachos and Kiratzi, 1992*; *Kiratzi and Papazachos, 1995*). In this study, the method developed by *Papazachos and Kiratzi (1992)* is used to quantify the coseismic deformation in the Gulf of Aqaba through the summation of seismic moment tensors. The method is based on the availability of seismicity parameters, focal mechanism solutions, and the maximum magnitude and dimensions of the seismogenic zone.

2. GEOLOGIC AND TECTONIC SETTING

The Gulf of Aqaba is one of two bifurcations at the northernmost end of the Red Sea that represent the NE-SW geologic trend in Egypt (*Makris and Henke, 1992*). Tectonic movements are younger in the Gulf of Aqaba than in the Gulf of Suez (*Lyberis, 1988*). The Gulf of Aqaba was formed in the Early or Middle Miocene orogeny (*Bosworth et al., 2005*) due to oblique drift of the Arabian plate combined with the opening of the Red Sea. Late Miocene motion is associated with a shear stress regime, characterized by extension in the direction of N40°E and compression in the direction of N130°E, which produced left-lateral motion between the Arabian plate and the Sinai subplate (*Lyberis, 1988*). Since the end of the Miocene, faulting has occurred due to the E-W extension, which indicates rotation of the regional stress pattern in the vicinity of the transform fault (*Lyberis, 1988*). Deformation along the Dead Sea Transform is characterized by 105 km of a sinistral slip in the direction of N25°E, which is typically accompanied by an extensional component

(*Garfunkel, 1981*). Landsat images reveal that the deformation extends only 20 km wide to the north and 60 km wide to the east around the coastlines of the Gulf (*Lyberi, 1988*).

Structurally, the Gulf of Aqaba is 180 km long and 25 km wide and formed from three successive pull-apart basins (*Garfunkel, 1981*). These basins are connected by en-echelon strike-slip faults with strikes of N20°E (*Ben-Avraham, 1985*) and accompanied by a small amount of extension that remains debatable (*Ben-Avraham and Zoback, 1992*). The pull-apart basins and the en-echelon strike-slip faults are shown in Fig. 2. Based on geophysical data, mantle upwelling is assumed in the region (*Ben-Avraham, 1997*). The velocity structure in the central part of the Gulf is postulated to be a transitional zone of oceanic crust, which is considered the most tectonically active part of the Gulf of Aqaba (*Ben-Avraham and Tibor, 1993*). Conversely, a continental crust structure is dominant in the northern part of the Gulf.

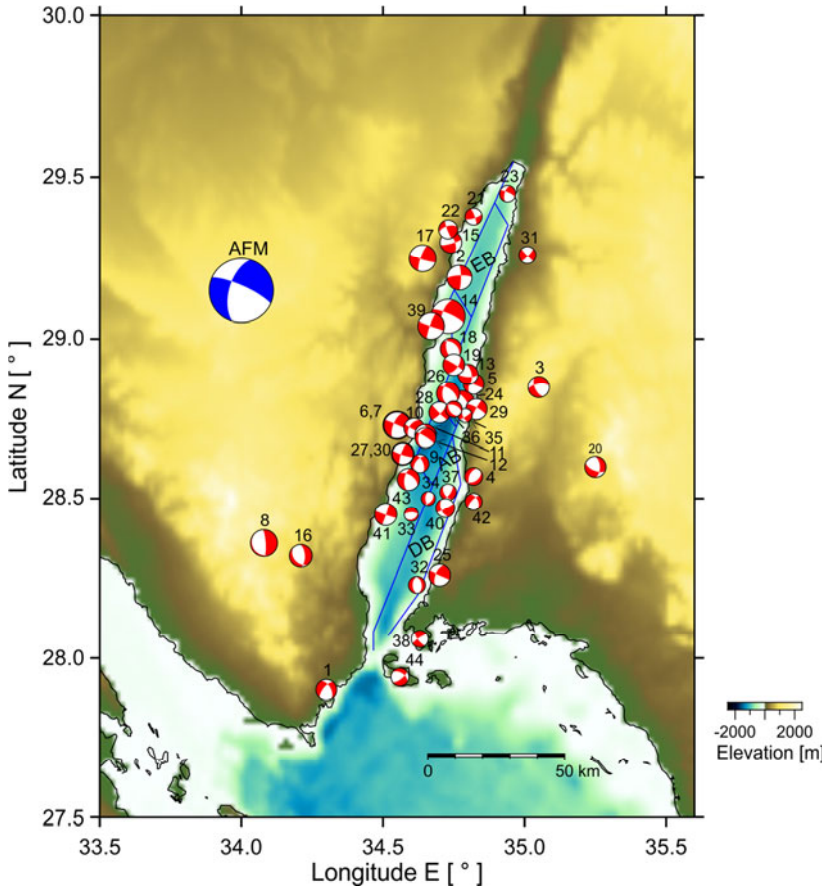

Fig. 2. Map of focal mechanism solutions (beach balls) listed with their IDs in Table 1. The average fault plane solution (AFM) obtained from moment-tensor summation is also shown. The pull-apart basins are given by the abbreviations: EB - the Elat basin, AB - the Aragonese basin, and DB - the Dakar basin. The solid curves represent the en-echelon strike-slip faults.

Despite the large 7.2 magnitude earthquake in 1995, the rate of seismicity in the Gulf is typically normal to low (*Klinger et al., 1999*). Seismic activity in the Gulf occurs in the 15 km thick upper crustal seismogenic zone between focal depths of 5 and 20 km (*Almadani, 2017*). Fault plane solutions reveal a dominant shear stress regime with sub-horizontal plunges for the maximum compressive stress (σ_1) and minimum compressive stress (σ_3), which are oriented northwest and northeast, respectively (*Hussein et al., 2013*).

3. MATERIALS AND METHODS

3.1. Data

In this study, the hypocenter parameters of past earthquakes were comprehensively collected and compiled into a homogeneous catalogue. Owing to the geographical location of the Gulf of Aqaba, the homogeneous catalogue was compiled using various earthquake catalogues published by the Institute of Petroleum Research and Geophysics (IPRG), *Abou Elenean (1997)*, the Egyptian National Seismological Network (ENSN), the Saudi Geological Survey, and the International Seismological Center (ISC). For this purpose, a unified moment magnitude was employed. The dataset used to estimate the seismic strain rate comprised 44 focal mechanism solutions of earthquakes with a moment-magnitude range of 3.2–7.2 collected from ISC. As well as data published by regional and international seismological centres, the dataset includes focal mechanism solutions published by *Badawy and Horváth (1999)*, *Hofstetter et al. (2003)*, *Salamon et al. (2003)*, *Hussein et al. (2013)*, *Mohamed et al. (2015)*, *Abdel-Aal and Badreldin (2016)*, *Badreldin et al. (2019)*, and *Ali and Badreldin (2019)*. The focal mechanism solutions are shown in Fig. 2 and the fault plane parameters for the corresponding earthquakes are listed in Table 1.

3.2. Methodology

In this study, the analysis method developed by *Papazachos and Kiratzi (1992)* was used. The method is based on the formulations of *Kostrov (1974)*, *Molnar (1979)*, and *Jackson and McKenzie (1988)*. The formula represents the average strain-rate tensor, as defined by *Kostrov (1974)*, and is given as follows:

$$\dot{\varepsilon}_{ij} = \frac{1}{2\mu V}\dot{M}_o \bar{F}_{ij}, \quad i,j = 1, 2, 3, \tag{1}$$

where V is the volume of the seismogenic deforming region and μ is the rigidity modulus, $\dot{M}_o$ is the annual scalar moment rate, and $\bar{F}_{ij}$ is the average shape tensor. The dimensions (length I_1, width I_2, and thickness I_3) of the deformed seismogenic zone were calculated from the distribution of seismicity using a simple least-squares technique (*Papazachos and Kiratzi, 1992*). Figure 1 shows that the seismogenic zone has a length of almost 150 km (I_1) and a width of 25 km (I_2). The thickness of 15 km (I_3) was determined from a depth-distance cross-section of the hypocenters. The azimuth of the deformation zone from the north is N20°E and the shear modulus is 3.0×10^4 Nm.

Table 1. The fault plane parameters of earthquakes used in the analysis. T_0: origin time, d: focal depth, M: magnitude, M_o: scalar seismic moment, M_w: moment magnitude, M_L: local magnitude.

ID	Date [yyyymmdd]	T_0 [s]	Long. [°]	Lat. [°]	d [km]	M	Strike [°]	Dip [°]	Rake [°]	M_o	M_w	Ref.
1	19820323	104800	27.90	34.30	10	4.7M_L	220	65.00	–40	4.42E+22	4.4	1
2	19830203	134604	29.19	34.77	24	5.3M_w	360	80.00	14	2.31E+23	5.3	2
3	19851231	194241	28.85	35.05	9	4.8M_L	155	60.00	–30	6.03E+22	4.5	1
4	19890909	0	28.57	34.82	10	4.1M_L	205	50.00	–110	6.84E+21	3.8	1
5	19930703	233410	28.86	34.82	18	4.7M_L	114	88.69	149	4.42E+22	4.4	3
6	19930803	4305	28.73	34.55	17	6.0M_w	7	62.00	–117	2.63E+24	6.0	4
7	19930803	124305	28.73	34.55	17	6.0M_L	294	87.27	–157	2.51E+24	5.6	3
8	19930803	163323	28.36	34.08	15	5.7M_L	356	79.41	–83	9.89E+23	5.7	3
9	19930807	45540	28.61	34.63	10	4.2M_L	217	50.19	–42	9.33E+21	3.9	3
10	19930820	230959	28.72	34.61	2	4.6M_L	116	79.84	140	3.24E+22	4.3	3
11	19931103	183932	28.70	34.65	7	4.9M_L	86	76.13	–148	8.22E+22	4.5	3
12	19931108	10602	28.69	34.65	8	4.7M_L	303	80.49	–120	4.42E+22	4.4	3
13	19931204	233411	28.89	34.80	10	4.6M_L	93	68.07	–148	3.24E+22	4.3	3
14	19951122	1526	29.07	34.73	18	7.2M_w	196	59.00	–15	1.71E+26	7.2	4
15	19951122	124704	29.30	34.74	15	5.0M_L	74	80.04	–150	1.12E+23	4.6	3
16	19951122	221657	28.32	34.21	15	5.2M_L	357	60.54	–69	2.09E+23	4.8	3
17	19951123	717	29.25	34.64	10	5.7M_w	199	77.00	7	9.27E+23	5.7	5
18	19951124	164345	28.97	34.74	10	4.9M_L	165	54.28	–68	8.22E+22	4.5	3
19	19951211	13208	28.92	34.75	19	5.0M_L	302	84.00	147	1.12E+23	4.6	3
20	19960103	100526	28.60	35.25	10	4.8M_L	113	59.77	–138	6.03E+22	4.5	3
21	19960108	1318	29.38	34.82	6	3.8M_L	340	78.86	164	2.69E+21	3.6	3
22	19960116	61700	29.34	34.73	6	4.3M_L	159	82.79	149	1.27E+22	4.0	3
23	19960204	72300	29.45	34.94	6	3.6M_L	294	77.43	–149	1.45E+21	3.4	3
24	19960221	5951	28.80	34.78	10	5.3M_w	132	30.00	–104	2.31E+23	5.3	5
25	19970510	147	28.26	34.70	10	4.6M_w	114	89.00	150	2.02E+22	4.6	4
26	20000308	142226	28.83	34.73	15	4.9M_w	182	48.00	–48	5.74E+22	4.9	4
27	20000308	122229	28.64	34.57	10	4.8M_w	198	31.00	–18	4.06E+22	4.8	4
28	20000308	142225	28.77	34.70	7	4.9M_L	135	85.10	–169	8.22E+22	4.5	3
29	20000406	63734	28.78	34.83	12	4.8M_L	209	85.10	–12	6.03E+22	4.5	3
30	20000803	142225	28.64	34.57	10	4.8M_L	108	82.31	167	6.03E+22	4.5	3
31	20010207	33900	29.26	35.01	21	3.6M_w	44	80.00	–5	6.25E+20	3.6	4
32	20021110	5945	28.23	34.62	16	3.9M_L	180	47.30	–84	3.67E+21	3.6	3
33	20040922	120023	28.45	34.60	10	3.2M_L	270	64.05	–76	4.17E+20	3.0	3
34	20050120	134100	28.50	34.66	19	3.2M_L	41	43.00	–56	4.17E+20	3.0	6
35	20080302	170600	28.76	34.79	14	3.2M_L	58	75.00	–29	4.17E+20	3.0	6

Table 1. Continuation.

ID	Date [yyyymmdd]	T_0	Long. [°]	Lat. [°]	d [km]	M	Strike [°]	Dip [°]	Rake [°]	M_o	M_w	Ref.
36	20080404	140500	28.78	34.75	7	$3.0M_L$	145	46.00	–67	1.97E+21	3.5	6
37	20111021	123700	28.52	34.73	9	$3.7M_L$	148	49.00	–147	1.97E+21	3.5	7
38	20130610	84400	28.06	34.63	6	$3.9M_L$	142	73.00	–15	3.67E+21	3.6	7
39	20150627	53404	29.04	34.67	22	$5.6M_w$	200	82.00	2	6.55E+23	5.6	5
40	20160516	14200	28.47	34.72	7	$4.3M_L$	157	52.00	–173	1.27E+22	4.0	8
41	20160516	4559	28.45	34.51	18	$5.2M_L$	19	88.00	–3	1.63E+23	4.7	4
42	20160813	30600	28.49	34.82	19	$3.9M_L$	332	47.00	–153	3.67E+21	3.6	8
43	20161129	113	28.56	34.59	18	$4.7M_w$	188	59.00	–44	2.86E+22	4.7	4
44	20170519	141600	27.94	34.56	4	$4.1M_L$	304	50.00	–27	6.84E+21	3.8	8

1 *Salamon et al. (2003)*
2 *Badawy and Horváth (1999)*
3 *Hussein et al. (2013)*
4 *International Seismological Centre (2020)*
5 Global Centroid Moment Tensor Catalog (https://www.globalcmt.org/CMTsearch.html, *Ekström et al., 2012*)
6 *Mohamed et al. (2015)*
7 *Abdel-Aal and Badreldin (2016)*
8 *Ali and Badreldin (2019)*

The annual scalar moment rate $\dot{M}_o$, as defined by *Molnar (1979)*, is based on the scalar moment of the largest earthquake observed in the zone ($M_{o,\,max}$), the Gutenberg-Richter constants (a and b), and the magnitude-moment (c and d) relations as follows:

$$\dot{M}_o = \frac{A}{1-B} M_{o,\,max}^{1-B}, \tag{2}$$

where

$$A = 10^{a+(bd/c)} \quad \text{and} \quad B = \frac{b}{c}.$$

The average shape tensor $\overline{F}_{ij}$ was then calculated as follows:

$$\overline{F}_{ij} = \frac{\sum_{n=1}^{N} M_o^n F_{ij}^n}{\sum_{n=1}^{N} M_o^n}, \tag{3}$$

where M_o^n and F_{ij} are the scalar seismic moment and the moment tensor for an individual event, respectively.

The elements of the moment tensor (F_{ij}) are a function of the strike, dip, and rake of the focal mechanism solution and the moment tensor is calculated using the equations defined by *Aki and Richards (1980)*. We introduce the following elements of the symmetric moment tensor (F_{ij}) for completeness:

$$\begin{aligned} F_{11} &= -\left(\sin\delta\cos\lambda\sin 2\phi + \sin 2\delta\sin\lambda\sin^2\phi\right), \\ F_{12} &= \sin\delta\cos\lambda\sin 2\phi + 0.5\sin 2\delta\sin\lambda\sin 2\phi, \\ F_{13} &= -\left(\cos\delta\cos\lambda\cos 2\phi + \cos 2\delta\sin\lambda\sin\phi\right), \\ F_{22} &= \sin\delta\cos\lambda\sin 2\phi - \sin 2\delta\sin\lambda\cos^2\phi, \\ F_{33} &= \sin 2\delta\sin\lambda, \end{aligned} \tag{4}$$

where φ, δ and λ are the strike, dip, and rake of the focal mechanism solution, respectively. Finally, based on the relationship developed by *Jackson and McKenzie (1988)*, the velocity tensor (U_{ij}) elements that are normal and parallel to the zone boundary, as well as vertical, are calculated using the following equations:

$$\begin{aligned} U_{11} &= \frac{1}{2\mu I_2 I_3}\dot{M}_o\bar{\bar{F}}_{11}, \quad U_{12} = \frac{1}{2\mu I_1 I_3}\dot{M}_o\bar{\bar{F}}_{12}, \quad U_{13} = \frac{1}{2\mu I_1 I_2}\dot{M}_o\bar{\bar{F}}_{13}, \\ U_{22} &= \frac{1}{2\mu I_1 I_3}\dot{M}_o\bar{\bar{F}}_{22}, \quad U_{23} = \frac{1}{2\mu I_1 I_2}\dot{M}_o\bar{\bar{F}}_{23}, \quad U_{33} = \frac{1}{2\mu I_1 I_2}\dot{M}_o\bar{\bar{F}}_{33}. \end{aligned} \tag{5}$$

As F_{ij} is calculated using the relations of *Aki and Richards (1980)*, a rotation of $\bar{\bar{F}}_{ij}$ in the reference system is required.

As proposed by *Papazachos and Kiratzi (1992)*, the Monte Carlo simulation technique is used to analyze the detailed errors in the strain-rate and velocity tensors. The influence of the tensor $\bar{\bar{F}}_{ij}$ introduced minimal uncertainties to the magnitude of deformation relative to the influence of the seismic moment rate $\dot{M}_o$. However, the direction of deformation was influenced by errors in tensor $\bar{\bar{F}}_{ij}$, whereas errors in $\dot{M}_o$ had no effect. The errors in $\dot{M}_o$ were measured by evaluating the errors in constants (*a, b, c*, and *d*) derived from the adopted Gutenberg-Richter law and the M_s-M_o relationship.

4. RESULTS

To quantify the rate of coseismic deformation, prior estimates of the Gutenberg-Richter and moment-magnitude relationships were performed. For this purpose, the homogeneous catalogue of unified moment magnitude was used. Seismicity in the Gulf of Aqaba has a maximum moment magnitude of 7.2 and moment-magnitude relation constants of $c = 1.5 \pm 0.04$ and $d = 15.36 \pm 0.20$, as determined by *Hofestetter (2003)*. Figure 3 shows the Gutenberg-Richter relation of seismicity parameters $a = 4.45 \pm 0.02$ and $b = 0.96 \pm 0.08$ for earthquakes with moment magnitudes of completeness of

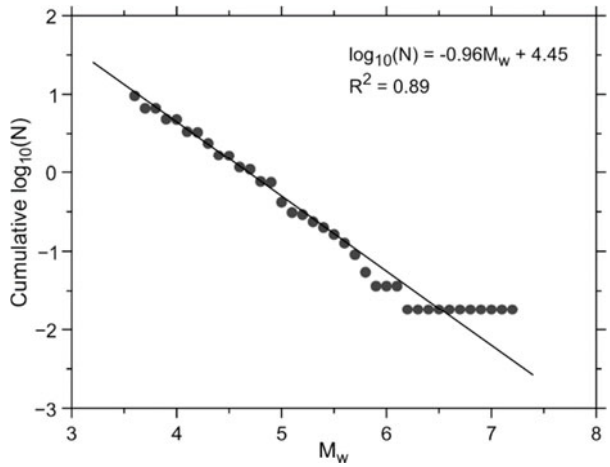

Fig. 3. Adopted Gutenberg-Richter law in the Gulf of Aqaba for a moment magnitude of completeness of 3.6 ± 0.14. The relationship was calculated using the maximum likelihood technique and uncertainties were determined using the bootstrapping statistical technique. M_W - moment magnitude, N – cumulative number of earthquakes.

3.6 ± 0.14, as determined in this study. Based on the constants derived from the adopted Gutenberg-Richter law and the constants of the moment-magnitude relationship, the scalar seismic moment rate $\dot{M}_o$ is 1.62×10^{17} Nm yr^{-1}.

By applying Eq. (3), the tensor $\overline{F}_{ij}$ for the Gulf of Aqaba is as follows:

$$\begin{bmatrix} -0.41 & 0.62 & 0.49 \\ 0.62 & 0.65 & 0.04 \\ 0.49 & 0.04 & -0.23 \end{bmatrix}.$$

The corresponding eigenvalues of the tensor $\overline{F}_{ij}$ are

$$\begin{bmatrix} \lambda^o & \varphi^o & \delta^o \\ 1.0 & 61.9 & 12.2 \\ -0.0 & 313.3 & 55.9 \\ -1.0 & 159.4 & 31.3 \end{bmatrix},$$

where λ^o represents the eigenvalues, φ^o is the azimuth, and δ^o is the plunge. The eigenvalues are ordered to represent the axes of minimum compressive stres (T), neutral, and maximum compressive stress (P) of the double couple focal mechanism. The formulation of *Papazachos and Kiratzi (1992)* is appropriate to minimize the influences of various focal mechanisms, where the focal mechanism solutions used in the present analysis ranged from strike-slip to normal faulting. The analysis reveals approximately

ideal values of the eigenvalues tensor of (1.0, 0.0, −1.0). The advantage of this formulation is that it takes into account the scalar seismic moment and the moment tensor shape of individual events. Based on the fault plane solutions used in this study, the eigensystem of tensor $\bar{F}_{ij}$ indicates that the Gulf of Aqaba is under a shear stress regime with a minor extensional component accommodated by ENE extension and almost NNW-SSE compression. The average focal mechanism exhibits a strike of 196.3°, a dip of 58.9°, and a rake of −14.8°, which indicates a sinistral strike-slip fault reveals that the composite moment tensor computed in this study is dominated by the earthquake of M_w 7.2.

Subsequently, using the values of the scalar seismic moment rate and tensor $\bar{F}_{ij}$ computed above, the components of both the strain-rate tensor ($\dot{\varepsilon}_{ij}$) and the velocity tensor (U_{ij}) were calculated by applying Eqs (1) and (5). The strain-rate tensor is as follows (components in 10^{-9} yr^{-1}):

$$\begin{bmatrix} 4.02 & 42.71 & 19.20 \\ 42.71 & 4.52 & -13.87 \\ 19.20 & -13.87 & -11.15 \end{bmatrix},$$

and the velocity tensor is (components in mm yr^{-1}):

$$\begin{bmatrix} 0.60 & 2.14 & 0.58 \\ 2.14 & 0.23 & -0.42 \\ 0.85 & -0.42 & -0.33 \end{bmatrix}.$$

The eigensystem of the velocity tensor is given as follows:

$$\begin{bmatrix} \lambda^o & \varphi^o & \delta^o \\ 2.6 \pm 0.04 & 42.2 & 2.9 \\ 0.1 \pm 0.01 & 133.2 & 22.4 \\ -2.0 \pm 0.02 & 305.2 & 67.4 \end{bmatrix}.$$

The dominant mode of coseismic deformation is approximately 42.71×10^{-9} yr^{-1} as expressed by the $\dot{\varepsilon}_{12}$ component of the strain-rate tensor, which indicates a left-lateral movement of the east and west sides. Notably, considerable vertical movement occurs at a rate of 11.22×10^{-9} yr^{-1}, which expresses crustal thinning. The eigensystem of the corresponding velocity tensor reveals that the Gulf of Aqaba is undergoing shear deformation accommodated by NE extension (N42.2°E) at a rate of 2.6 ±0.04 mm yr^{-1} and almost NW-SE compression (N305.2°E) at a rate of 2.0 ±0.02 mm yr^{-1}, reflecting predominantly left-lateral strike-slip faulting with a strike of 175.5°, a dip of 72.3°, and a rake of −14.2° (Fig. 4). The standard deviations associated with the solution were calculated using the approach proposed by *Papazachos and Kiratzi (1992)*, which considers the possible random errors of the model parameters using a Gaussian noise

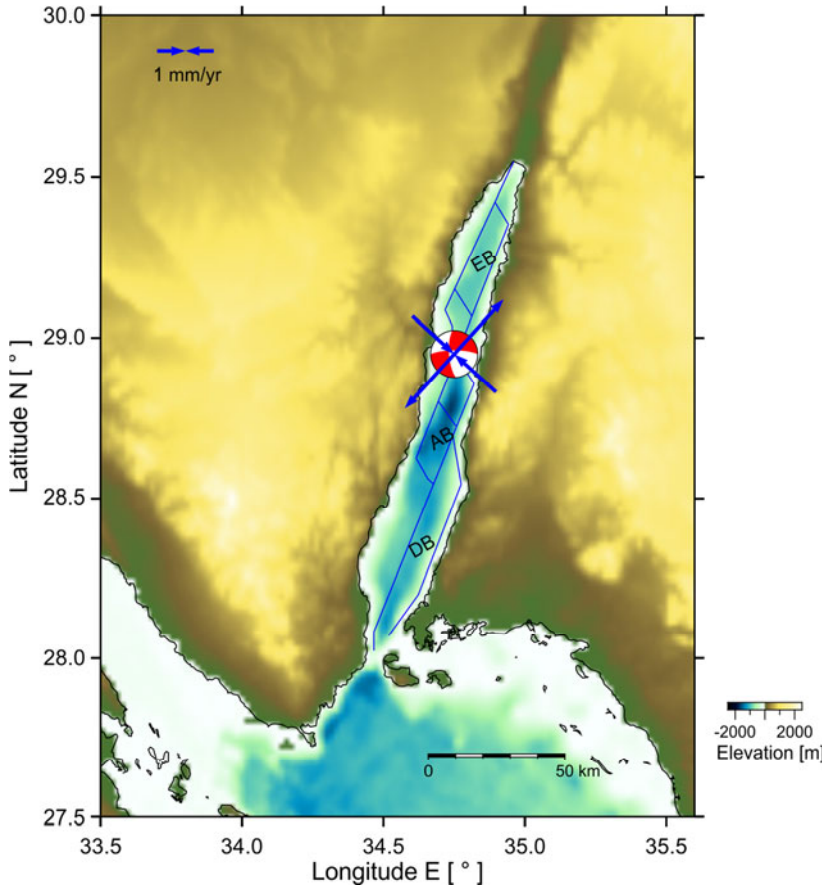

Fig. 4. Stress regime and the corresponding focal mechanism in the Gulf of Aqaba as derived from the velocity tensor. Arrows denote the rate of coseismic deformation. The pull-apart basins (EB - the Elat basin, AB - the Aragonese basin, and DB - the Dakar basin) and the en-echelon strike-slip faults (solid curves) are shown.

generator. New random parameters generated in each iteration were used to estimate the alternative values of $\dot{M}_o$, as well as the corresponding strain and velocity tensors. The random values within the mean standard errors were used to obtain reasonable uncertainties where the error factor of the constants of the Gutenberg-Richter law and M_S-M_O relationship account for approximately three.

5. DISCUSSION AND CONCLUSIONS

The seismic moment-tensor summation technique followed in this study is useful for deepening our understanding of the deformation caused by seismic slips along plate

boundary zones. The Gulf of Aqaba represents the southernmost segment of the Dead Sea Transform Fault, which is characterized by shear deformation accompanied by an extensional stress regime that led to the formation of pull-apart basins. The most intense seismicity in the Gulf of Aqaba exhibits a direct relationship with the northward motion of the Arabian plate relative to the African plate, with an anticlockwise rotation of 6° at a rate of 10 mm yr^{-1} (*Girdler, 1966*; *Garson and Krs, 1976*). Moreover, anticlockwise rotation of the Sinai subplate toward the northwest with respect to the Arabian plate plays a key role in the present-day tectonic deformation in the Gulf of Aqaba.

The moment-tensor summation technique was used to quantify the magnitude and vector direction of deformation characterizing the studied zone. A total of 44 fault plane solutions, the adapted Gutenberg-Richter law, and the moment-magnitude relationship were used to estimate the seismic strain tensor magnitudes and directions. The scalar moment rate of earthquakes that occurred in the area from 1964–2019 is equal to 1.62×10^{17} Nm yr^{-1}. The deformation is accommodated by maximum compressive stress, P-axis, which has approximately shallow plunge of 22.4° toward N133.2°E, and minimum compressive stress, T-axis, which has a shallow horizontal plunge of 2.9° toward N42.2°E, corresponding to the coupling between an extensional stress regime that activated an approximately left-lateral strike-slip focal mechanism with a normal component (strike 175.5°, dip 72.3°, and rake −14.2°). The results obtained from this study reveal a deformation pattern related to relative plate motion between the African and Arabian plates, as well as the key role played by the relative motion of the Sinai subplate. Owing to the relative motions between continental plates in this region, coseismic deformation in the Gulf of Aqaba region is consistent with a tectonic process that coupled the prevailing tensional stress with left-lateral strike-slip movement. Based on the analysis of 44 earthquakes with moment magnitudes in the range of 3.2–7.2, the focal mechanism solutions alternated between strike-slip and normal faulting mechanisms, which reflect the various processes involved in the transition from rifting in the north Red Sea to continental transform in the Gulf of Aqaba and the Dead Sea. Notably, previous seismic tomography analysis revealed no transition of oceanic crust into the Gulf (*El Khrepy, 2016*). The majority of the focal mechanism solutions reveal strike-slip movement with a normal component, which could be attributed to the NNE left-lateral strike-slip faults parallel to the Gulf. Normal faulting mechanisms are attributed to nine earthquakes, which reflect the transverse NNW–SSE faults that form the boundaries of major basins in the Gulf (*Salamon et al., 2003*).

The results of the velocity tensor obtained from this study indicate that the present-day stress regime is left-lateral strike-slip deformation with a reverse component accommodated along the NNW–SSE trending plane; these are relatively consistent with the results deduced from the stress tensor inversion by *Hussein et al. (2013)*, which revealed maximum compressive stress, σ_1, with a plunge of 19° ± 11° towards N145° ± 13°E and minimum compressive stress, σ_3, with a shallow horizontal plunge of 1° ± 5° toward N56° ± 15°E. Alternatively, the results obtained by *Ali and Badreldin (2019)* exhibited significant differences, i.e., the maximum compressive stress, σ_1, has a plunge of 23° ± 15° toward N357° ± 46°E and the minimum compressive stress, σ_3, has a shallow horizontal plunge of 8° ± 2° toward N90° ± 49°E. The uncertainties indicate the

differences between these results. By repeating the calculations using datasets of focal mechanisms published by *Hussein et al. (2013)*, the coseismic deformation in the Gulf of Aqaba is characterized by an average extension of 0.95 ± 0.2 yr^{-1} with a mean direction of N35.6° ± 7.2°E.

The analysis of GPS measurements in the area revealed that the rate of crustal deformation of the Gulf of Aqaba is 3.2 mm yr^{-1} to the north and 1.8 mm yr^{-1} to the east (*Mahmoud et al., 2005*; *Reilinger et al., 2006*). The slip rate retrieved from geodetic measurements showed left-lateral deformation of 4.4 ± 0.3 mm yr^{-1} in the Gulf of Aqaba-Dead Sea Transform Fault (*Mahmoud et al., 2005*), whereas the sinistral motion of 5.6 ± 1.0 mm yr^{-1} was determined for the southernmost segment of the Aqaba fault (*McClusky et al., 2003*). The low recurrence rate of earthquakes with magnitudes greater than six implied that the total horizontal slip rate of 2–4 mm yr^{-1} is accommodated along the Gulf of Aqaba (*Makovsky et al., 2008*). It is noteworthy that four events with magnitudes greater than 6.5 occurred within a period of 2000 years, indicating a maximum velocity of approximately 4 mm yr^{-1} for the cumulative displacement of approximately 8 m (*Klinger et al., 1999*). Conversely, the velocity derived from regional kinematic plate tectonics models is approximately 7.5–9.5 mm yr^{-1} (e.g., *Jestin et al., 1994*), suggesting a normal level of seismicity compared with that predicted by plate tectonics models. Interestingly, the results of this study reveal a well consistent rate of coseismic deformation with the aforementioned studies in the Gulf of Aqaba. The resulted deformation characterized by an extension rate of 2.6–0.04 mm yr^{-1} along the direction of N42.2°E and vertical deformation of 2.0–0.02 mm yr^{-1} along the direction of N305.2°E that implies a dominant shear deformation. Contrary, in the Gulf of Suez the coseismic deformation is expressed by extension at a rate of 0.008 mm yr^{-1} in the direction of N28°E with crustal thinning of 0.0034 mm yr^{-1} (*El-Nader and Hussein, 2018*), indicating small coseismic deformation relative to that in the Gulf of Aqaba.

Thus, the dominant mode of coseismic deformation in the Gulf of Aqaba is the east-west extension and north-south compression at 2.6–0.04 mm yr^{-1} and 2.0–0.02 mm yr^{-1}, respectively. Small vertical movement at a rate of 0.33 mm yr^{-1} was also observed, that might correspond to crustal thinning due to a potential transition of oceanic crust into the Gulf imported from the Red Se rifting. The results of this study imply that interaction between the relative tectonic motions of the African and Arabia plates, as well as the key role of Sinai subplate, is responsible for the present-day crustal deformation in the Gulf of Aqaba. It is noteworthy to mention that Late Miocene motion associated with a shear stress regime of extension toward N40°E and compression toward N130°E produced left-lateral motion between the Arabian plate and the Sinai Peninsula (*Lyberis, 1988*).

Acknowledgements: This work was supported by the King Saud University Deanship of Scientific Research, College of Science Research Centre. Generic Mapping Tools developed by *Wessel and Smith (1991)* were used for data mapping.

References

Abdel-Aal K. and Badreldin H., 2016. Seismological aspects of the 27 June 2015 Gulf of Aqaba earthquake and its sequence of aftershocks. *J. Seismol.*, **20**, 935–952.

Abdel-Fattah A.K., Hussein H.M. and El-Hady S., 2006. Another look at the 1993 and 1995 Gulf of Aqaba earthquakes from the analysis of teleseismic waveforms. *Acta Geophys.*, **54**, 260–279.

Aki K. and Richards P.G., 1980. *Quantitative Seismology: Theory and Methods*. W.H. Freeman and Co., San Francisco, CA.

Ali S.M. and Badreldin H., 2019. Present-day stress field in Egypt based on a comprehensive and updated earthquake focal mechanisms catalog. *Pure Appl. Geophys*., **176**, 4729–4760.

Almadani S., 2017. Source parameters of the 27th of June 2015 Gulf of Aqaba earthquake. *J. Seismol.*, **21**, 1055–1066.

Badawy A. and Horváth F., 1999. Recent stress field of the Sinai subplate region. *Tectonophysics*, **304**, 385–403.

Badreldin H., Toni M. and El-Faragawy K., 2019. Moment tensor inversion of small-to-moderate size local earthquakes in Egypt. *J. Afr. Earth Sci.*, **151**, 153–172.

Ben-Avraham Z. and Tibor G., 1993. The northern edge of the Gulf of Elat. *Tectonophysics*, **226**, 319–331.

Ben-Avraham Z. and Zoback M.D., 1992. Transform-normal extension and asymmetric basins: An alternative to pull-apart models. *Geology*, **20**, 423–426.

Ben-Avraham Z., 1985. Structural framework of the Gulf of Elat (Aqaba), northern Red Sea. *J. Geophys. Res.-Solid Earth*, **90**, 703–726.

Ben-Avraham Z., Hartnady C.J.H. and Kitchin K.A., 1997. Structure and tectonics of the Agulhas-Falkland fracture zone. *Tectonophysics*, **282**, 83–98.

Bosworth W., Huchon P. and McClay K., 2005. The red sea and gulf of Aden basins. *J. Afr. Earth Sci*., **43**, 334–378.

Daggett P.H., Morgan P., Boulous F.K., Hennin S.F., El-Sherif A.A., El-Sayed A.A., Basta N.Z. and Melek Y.S., 1986. Seismicity and active tectonic of the Egyptian Red Sea margin and the northern Red Sea. *Tectonophysics*, **125**, 313–324.

El Khrepy S., Koulakov I., Al-Arifi N. and Petrunin A.G., 2016. Seismic structure beneath the Gulf of Aqaba and adjacent areas based on the tomographic inversion of regional earthquake data. *Solid Earth*, **7**, 965–978.

El-Nader I.A. and Hussein H.M., 2018. The present-day active deformation in the central and northern parts of the Gulf of Suez area, Egypt, from earthquake focal mechanism data. *Nat. Hazards*, **92**, 1355–1369.

Ekström, G., M. Nettles, and A. M. Dziewonski, 2012. The global CMT project 2004-2010: Centroid-moment tensors for 13,017 earthquakes, Phys. Earth Planet. Inter., 200-201, 1-9, DOI: 10.1016/j.pepi.2012.04.002

Garson M.S. and Krs M., 1976. Geophysical and geological evidence of the relationship of Red Sea transverse tectonics to ancient fractures. *Bull. Geol. Soc. Amer.*, **87**, 169–181.

Garfunkel Z., 1981. Internal structure of the Dead Sea leaky transform (rift) in relation to plate kinematics. *Tectonophysics*, **80**, 81–108.

Girdler R.W., 1966. The role of translational and rotational movement in the formation of the Red Sea and Gulf of Aden. In: *The World Rift System*. Geological Survey of Canada, Canada Paper 66-14, 65–77.

Hofstetter A., 2003. Seismic observations of the 22/11/1995 Gulf of Aqaba earthquake sequence. *Tectonophysics*, **369**, 21–36.

Hussein H.M., Elenean K.A., Marzouk I.A., Korrat I.M., El-Nader I.A., Ghazala H. and ElGabry M.N., 2013. Present-day tectonic stress regime in Egypt and surrounding area based on inversion of earthquake focal mechanisms. *J. Afr. Earth Sci.*, **81**, 1–15.

International Seismological Centre, 2020. *On-line Bulletin*, DOI: 10.31905/D808B830 (http://www.isc.ac.uk/iscbulletin/search/fmechanisms/).

Jackson J. and McKenzie D., 1988. The relationship between plate motions and seismic moment tensors, and the rates of active deformation in the Mediterranean and Middle East. *Geophys. J. Int*., **93**, 45–73.

Jestin F., Huchon P. and Gaulier J.M., 1994. The Somalia plate and the East African Rift System: present-day kinematics. *Geophys. J. Int*., **116**, 637–654.

Lyberis N., 1988. Tectonic evolution of the Gulf of Suez and the Gulf of Aqaba. *Tectonophysics*, **153**, 209–220.

Kiratzi A.A. and Papazachos C.B., 1995. Active crustal deformation from the Azores triple junction to the Middle East. *Tectonophysics*, **243**, 1–24.

Kiratzi A.A. and Langston C.A., 1991. Moment tensor inversion of the 1983 January 17 Kefallinia event of Ionian islands (Greece). *Geophys. J. Int*., **105**, 529–535.

Kiratzi A.A., 1993. A study on the active crustal deformation of the North and East Anatolian Fault Zones. *Tectonophysics*, **225**, 191–203.

Klinger Y., Rivera L., Haessler H. and Maurin J.-C., 1999. Active faulting in the Gulf of Aqaba: new knowledge from the Mw 7.3 Earthquake of 22 November 1995. *Bull. Seismol. Soc. Amer*., **89**, 1025–1036.

Kostrov V.V., 1974. Seismic moment and energy of earthquakes, and seismic flow of rock. *Izv. Acad. Sci. USSR Phys. Solid Earth*, **1**, 23–44.

Makovsky Y., Wunch A., Ariely R., Shaked Y., Rivlin A., Shemesh A., Avraham Z.B. and Agnon A., 2008. Quaternary transform kinematics constrained by sequence stratigraphy and submerged coastline features: the Gulf of Aqaba. *Earth Planet. Sci. Lett*., **271**, 109–122.

McCloskey J., Nalbant S.S., Steacy S., Nostro C., Scotti O. and Baumont D., 2003. Structural constraints on the spatial distribution of aftershocks. *Geophys. Res. Lett.*, **30**, Art.No. 1610, DOI: 10.1029/2003GL017225.

Mahmoud S., Reilinger R., McClusky S., Vernant P. and Tealeb A., 2005. GPS evidence for northward motion of the Sinai block: implications for E. Mediterranean tectonics. *Earth Planet. Sci. Lett*., **238**, 217–227.

Mohamed E.K., Hassoup A., Abou Elenean K.M., Othman Adel A.A. and Hamed Diaa-Eldin M.K., 2015. Earthquakes focal mechanism and stress field pattern in the northeastern part of Egypt. *NRIAG J. Astron. Geophys.*, **4**, 205–221.

Makris J. and Henke C. H., 1992. Pull-apart evolution of the Red Sea. *J. Pet. Geol.*, **15**, 127–134.

Molnar P., 1979. Earthquake recurrence intervals and plate tectonics. *Bull. Seismol. Soc. Amer.*, **69**, 115–133.

Papanikolaou I.D., Roberts G.P. and Michetti A.M., 2005. Fault scarps and deformation rates in Lazio-Abruzzo, central Italy: Comparison between geological fault slip-rate and GPS data. *Tectonophysics*, **408**, 147–176.

Papazachos C.B. and Kiratzi A.A., 1992. A formulation for reliable estimation of active crustal deformation and its application to central Greece. *Geophys. J. Int.*, **111**, 424–432.

Reilinger R., McClusky S., Vernant P., Lawrence S., Ergintav S., Cakmak R., Ozener H., Kadirov F., Guliev I., Stepanyan R. and Nadariya M., 2006. GPS constraints on continental deformation in the Africa-Arabia-Eurasia continental collision zone and implications for the dynamics of plate interactions. *J. Geophys. Res.-Solid Earth*, **111**, Art.No. B05411, DOI: 10.1029/2005JB004051.

Salamon A., Hofstetter A., Garfunkel Z. and Ron H., 1996. Seismicity of the eastern Mediterranean region: perspective from the Sinai subplate. *Tectonophysics*, **263**, 293–305.

Salamon A., Hofstetter A., Garfunkel Z. and Ron H., 2003. Seismotectonics of the Sinai subplate - the eastern Mediterranean region. *Geophys. J. Int*., **155**, 149–173.

Visini F., de Nardis R. and Lavecchia G., 2010. Rates of active compressional deformation in central Italy and Sicily: evaluation of the seismic budget. *Int. J. Earth Sci*., **99**, 243–264.